Detailed Validation of Numerical Simulations of Air-blast Spray Atomization against Experimental Back-lit Images and Radiographs

Lam Vu*[1], Nathanaël Machicoane[2,4], Danyu Li[3], Timothy Morgan[3], Theodore J. Heindel[3], Alberto Aliseda[2], Olivier Desjardins[1]

[1]1Department of Mechanical and Aerospace Engineering, Cornell University, Ithaca, USA
[2]Department of Mechanical Engineering, University of Washington, Seattle, USA
[3]Department of Mechanical Engineering, Iowa State University, Ames, USA
[4]Univ. Grenoble Alpes, CNRS, Grenoble INP, LEGI, 38000 Grenoble, France
*Corresponding author email: lxv2@cornell.edu

Abstract

Sprays appear in a variety of industrial applications ranging from powder production used in additive manufacturing to fuel nozzles. Air-blast atomization is a specific injection strategy whereby a high-speed gas shears and destabilizes a low-speed liquid which causes a cascade of instabilities leading to the creation of a spray. The flow physics around the nozzle are challenging to quantify and complex. Inside the nozzle, traditional PIV and hot-wire methods cannot be used to measure turbulence and boundary layer growth and at the nozzle exit, radiographs and back-lit images show complex time-varying wetting and contact line dynamics. In this study, we explore different computational strategies to model these flow physics and validate them against equivalent path length data (EPL), a measure of the liquid depth along a line-of-sight. Further downstream, thin liquid structures that fall below the mesh size are prone to numerical break-up and as a consequence, we employ a thin-film model to improve agreement. We make use of a multi-block simulation strategy to address the multi-scale nature of atomization. Finally, using these models, we make direct comparisons of quantities such as the liquid intact length.

Introduction

Air-blast atomization is a complex process whereby a high-speed gas shears a low-speed liquid, triggering a cascade of instabilities that break up the liquid into a collection of drops which form a spray. This atomization strategy is used in numerous engineering applications such as metal powder production for additive manufacturing, sprays for medical coatings, and fuel injection for gas turbine engines. Understanding the spray formation and dispersion process is crucial for design of fuel efficient and low pollutant emitting combustion systems.

Air-blast atomization has been studied extensively using experimental back-lit imaging and shadowgraphy techniques. These experimental measurements have resulted in useful engineering tools such as regime maps of swirl number and momentum flux ratio [1], liquid entrainment models that well predict liquid ligament shedding frequency [2], and correlations for liquid longitudinal wavelength and transverse corrugation sizes [3]. Most recently, X-ray imaging utilizing specialized facilities at Argonne National Lab's Advanced Photon Source has been used successfully to visualize 3D structures in the flow, enabling the study of physics like bubble entrainment and contact line dynamics [4, 5]. The wide range of length scales in air-blast atomization, starting from the large combustion chamber and nozzle scales, down to the small interfacial and turbulence scales, have made simulations challenging. One method to circumvent the need to simulate the internal flow of the nozzle is to make use of analytical models for the velocity profile just downstream of the nozzle exit, as is classically used in linear stability analysis [6]. Just past the nozzle exit, the initial destabilization of the liquid leads to complex interface dynamics and frequent topology change. Dual grid methods where the phase tracking equations are solved on a refined mesh formed around the interface [7] and AMR block

strategies where mesh resolution is concentrated around the interface [8], have been used successfully in addressing this challenge but often require complex dynamic meshing. Further downstream, the dense cloud of drops formed by the spray become too computationally demanding to simulate and typically, these drops are converted into a simpler collection of Lagrangian particles and tracked using traditional particle methods [9, 10].

Our strategy is a pragmatic approach where the momentum and phase transport equations are solved on the same Eulerian Cartesian mesh. The disparity of length scales in the problem is addressed using a multi-block strategy whereby separate simulations, or blocks, purposed for their respective length scale, are coupled through boundary conditions while small length scales are addressed using sub-grid scale (SGS) models. In this study, the first block is a single-phase simulation of the gas flow inside the nozzle and the second block is a more refined simulation of the atomization region. This multi-block strategy can be generalized and naturally permits a third block to be added where detached sheets, ligaments, and drops, resulting from second block, can be converted into Lagrangian particles and tracked. We employ a sub-grid scale contact line model to allow the interface to travel freely along the nozzle tip and a thin film model to track liquid structures with length scales below the mesh size. Simpler simulation configurations without the multi-block strategy and the sub-grid scale models are also presented to show the effectiveness of the described tools. To complement this work, we validate the results against state-of-the-art X-ray equivalent path length data and back-lit imaging.

Numerical Methods

We consider liquid-gas flows governed by the continuity equation

$$\frac{\partial \rho}{\partial t} + \nabla \cdot (\rho \mathbf{u}) = 0 \tag{1}$$

and the incompressible Navier-Stokes equation

$$\frac{\partial \rho \mathbf{u}}{\partial t} + \nabla \cdot (\rho \mathbf{u}\mathbf{u}) = -\nabla p + \nabla \cdot \left(\mu \left[\nabla \mathbf{u} + \nabla \mathbf{u}^{\mathsf{T}}\right]\right) + \rho \mathbf{g}, \tag{2}$$

where ρ is the fluid density, μ is the dynamic viscosity, $\mathbf{u}$ is the velocity, p is the pressure, $\mathbf{g}$ is the gravitational acceleration, and t is time. Fluid properties are constant within each phase but differ between the phases. We use subscripts l and g to denote liquid and gas quantities, respectively. If Γ indicates the interface and $\left[\ \right]_\Gamma$ indicates the jump of a property across the interface, then the jump in density and viscosity across the interface are $\left[\rho\right]_\Gamma = \rho_l - \rho_g$ and $\left[\mu\right]_\Gamma = \mu_l - \mu_g$, respectively. The velocity is continuous across the interface, hence $\left[\mathbf{u}\right]_\Gamma = 0$, and the pressure jump across the interface is given by

$$\left[p\right]_\Gamma = \sigma\kappa + 2\left[\mu\right]_\Gamma \mathbf{n}^{\mathsf{T}} \cdot \nabla \mathbf{u} \cdot \mathbf{n}, \tag{3}$$

where σ is the surface tension coefficient, κ is the interface curvature, and $\mathbf{n}$ is the interface normal. The equations are solved using an in-house, conservative, finite volume flow solver for low Mach number flows [11]. Phase tracking is handled with a geometric, semi-Lagrangian Volume-of-Fluid method [12]. This solver is second-order accurate in time and space and, away from the interface, is discretely kinetic energy conserving. Inside each computational cell, the interface is represented locally as a plane using piece-wise linear interface reconstruction (PLIC) with the plane normal calculated using LVIRA [13]. To capture sub-grid scale effects, a dynamic Smagorinsky turbulence model [14], a thin-film capturing model based on R2P [15], and sub-grid scale contact line model are employed [16]. The curvature of the interface is calculated using parabolic surface fits. The pressure jump due to this curvature is then embedded as a source term in the pressure Poisson equation using a continuous surface approach [17].

Experimental Methods

A canonical coaxial two-fluid atomizer is used for the experimental investigations. Air flows through 4 inlets perpendicular to the nozzle axis, and along converging cubic-spline shaped inner and outer walls to form a round annular turbulent jet, around a laminar circular water jet. The inner wall separating liquid and gas streams has an inner and outer dimension of d_l and D_l while the outer wall has an inner and outer dimension of d_g and D_g. x denotes the downstream direction while y and z are the perpendicular directions. The near-field of the atomizer is characterized using visible light at University of Washington and synchrotron X-rays at the Advanced Photon Source of Argonne National Laboratory. In the former, high spatial and temporal resolution back-lit imaging is considered, yielding almost binary images indicating liquid presence, where simple thresholding can be used to identify the liquid interface's time evolution [5]. In the latter, EPL is measured using a focused monochromatic X-ray beam [4].

Simulation Set-up

To study the near-field region, we perform simulations of air-blast atomization in the same canonical nozzle using water and air properties. We consider one experimental condition at a gas Reynolds number, $Re_g \equiv 4Q_{Total}/\sqrt{4\pi A_g}\nu_g$, of 21400, a liquid Reynolds number, $Re_l \equiv \rho_l U_l d_l/\mu_l$, of 1200, a momentum flux ratio, $M \equiv (\rho_g U_g^2)/(\rho_l U_l^2)$, of 6.4, and a Weber number, $We \equiv \rho_g(U_g - U_l)^2 d_l/\sigma$, of 39.1 where Q_{Total} is the total gas flow-rate, A_g is the gas flow-through area, ν_g is the gas kinematic viscosity and U_g and U_l are the gas and liquid bulk velocities, respectively. We present four simulations at this condition with various configurations in order of increasing complexity. In all cases, the laminar liquid jet is prescribed with a parabolic velocity profile and the gas jet is at a sufficiently high Reynolds number that a dynamic sub-grid scale turbulence model is needed and employed. To reduce computational cost, the atomization simulations in case 1 and 2 are performed without the nozzle, as shown in figure 1, requiring an inflow model at the nozzle exit plane. In both cases, a fully developed annular pipe flow at the same gas Reynolds number is used for the gas inflow conditions. The inner wall separating the liquid and gas streams, the splitter plate, is modeled as a 0 velocity gas in case 1, implying the interface is pinned at d_l, and modeled as a 0 velocity liquid in case 2, implying the interface is pinned at D_l. Case 3 and 4 include the geometry of the nozzle in the calculation but are solved on a separate grid, block 1, and provide boundary conditions for the atomization simulation, block 2 as illustrated in figure 1. The overlap region between the two blocks is sufficiently large to justify the one way coupling from block 1 onto block 2. In both cases, a SGS contact line model with a static contact angle of $70°$ is used to allow the contact line to move freely and in case 4, a thin-film model is used to capture thin sheets that fall below the mesh resolution. All meshes are Cartesian and the converging nozzle walls are created by stair-stepping full cells that are treated as solid boundaries. Case 1 and 2 have uniform mesh resolution in all directions with a mesh size of $\Delta/d_l = 0.042$. For case 3 and 4, block 1 has uniform resolution in all directions with a size of $\Delta/d_g = 0.05$ and block 2 has uniform resolution in all directions with a size of $\Delta/d_l = 0.1$. The cases are summarized in table 1.

The corresponding radial gas velocity profiles, averaged in time and in θ, are shown in figure 2. Without any liquid present, the experimental gas velocity profiles are measured a small distance downstream of the nozzle using hot-wires. Because of the mismatch between conditions and measurement location, the comparison of velocity between simulations and experiments is mostly qualitative. The nozzle simulation better agrees with the experimental measurements than the annular turbulent pipe flow. The annular turbulent pipe flow produces a boundary layer thickness and fluctuations larger than both the nozzle simulation and experiments.

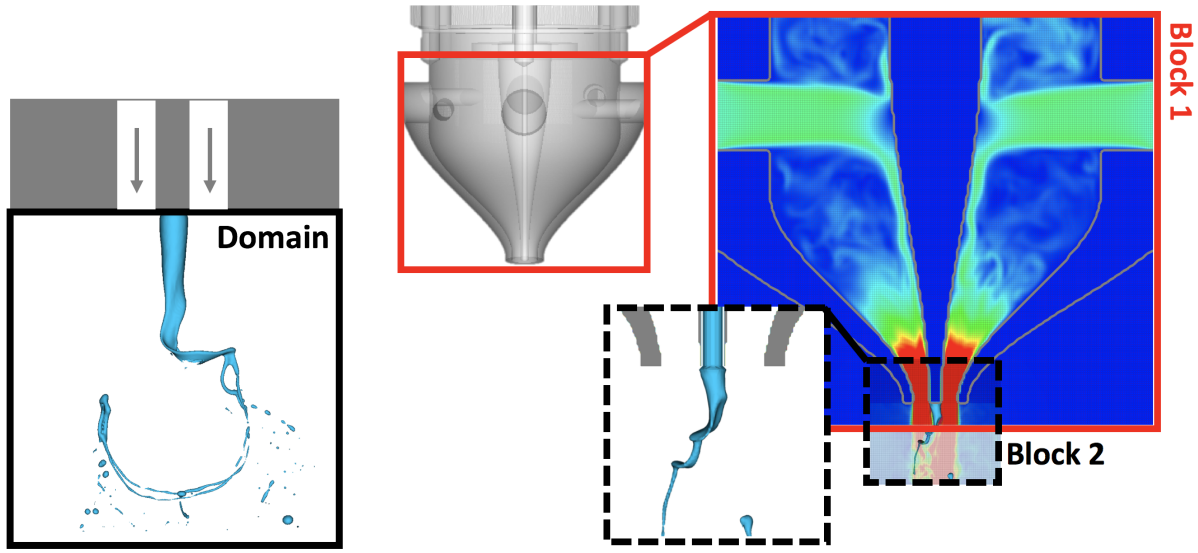

(a) Case 1 and 2

(b) Case 3 and 4

Figure 1. Illustration of computational set up. a) Domain excludes the nozzle and utilizes an annular pipe flow to model the gas velocity b) Multi-block strategy where block 1 models the internal nozzle flow and block 2 models the atomization.

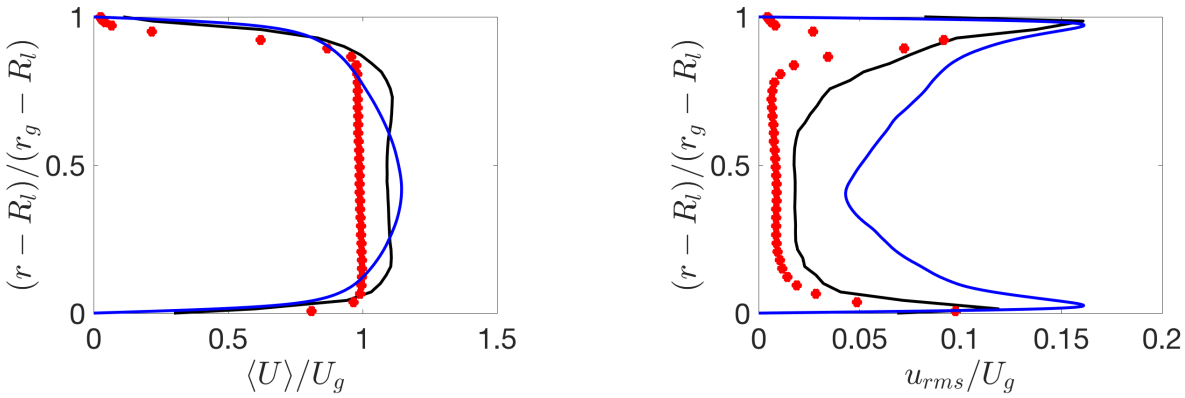

Figure 2. Comparison of velocity statistics. $R_l = 0.5D_l$ and $r_g = 0.5d_g$. Experiment (•), Annular pipe (——), Nozzle Flow(——).

Results and Discussion

Simulations are validated against experimental measurements of equivalent path length (EPL), a line-of-sight integration of liquid depth, obtained from focused monochromatic X-ray beam data. The EPL sampled along x, at the centerline ($y = 0$), gives a measure of the approximate liquid diameter as a function of the downstream distance and spatially quantifies how coherent the liquid is. Comparisons between simulations and experiments of this quantity are made in figure 3.

Case 1, where the splitter plate at the exit plane is modeled as a 0 velocity gas, is a seemingly straight-forward model since, without any flow, this region is the intersection between solid metal and static gas. This model implies that the interface pins at the inner edge of the splitter plate, d_l. As the liquid enters the domain, the combination of this pinning and the 0 velocity gas region forces the liquid to expand until the interface reaches the high-speed gas stream at $x \approx 0.25D_L$, as seen in figure 3 and it is only after this point that the liquid begins to destabilize. This phenomenon shifts the instabilities far downstream. In the experimental X-ray imaging, it is observed that the interface dynamically wets the splitter plate and in some instances, can even wick up along the gas inner wall at D_l. In case 2, the splitter plate is

Table 1. Summary of simulation configurations: $Re_g = 21400, Re_l = 1200$, $M = 6.4, We = 39.1$

Case	Gas Profile	Interface Boundary Condition	SGS Model
1	Annular turbulent pipe	Pinned at d_l	Turbulence model
2	Annular turbulent pipe	Pinned at D_l	Turbulence model
3	Block 1: nozzle simulation	Free with a static contact angle of $70°$	Turbulence, contact line model
4	Block 1: nozzle simulation	Free with a static contact angle of $70°$	Turbulence, contact line, thin-film model

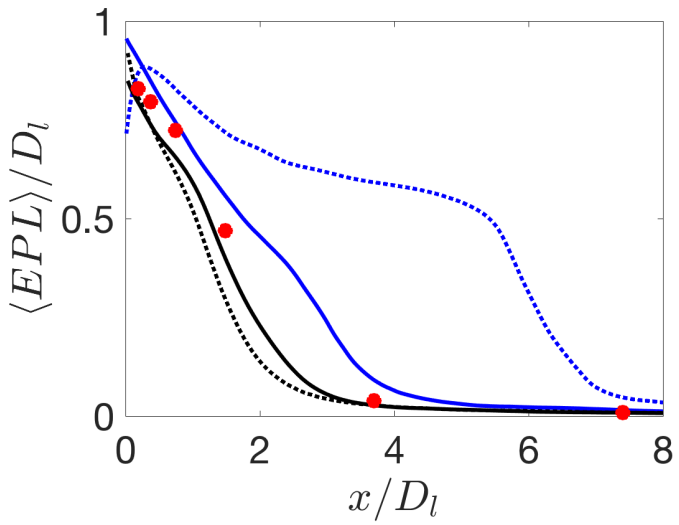

Figure 3. Centerline EPL profiles. Experiment (•), Case 1 (·····), Case 2 (——), Case 3 (·····), Case 4 (——).

modeled as a 0 velocity liquid; this pins the interface to the outer edge of the splitter plate, D_l, and brings the interface closer to the high-speed gas stream which more closely matches the experimental conditions. The resulting centerline EPL from this case decreases monotonically and is in better agreement with the experiments than in case 1. However, it still remains more stable than the experiment, possibly because of the pinned interface. Case 3 simulates the internal nozzle flow and makes use of a sub-grid scale contact line model which allows for a free moving contact line. These two factors result in a liquid that destabilizes faster than case 2 and the experiment. Figure 4 shows that with a single interface reconstruction method (PLIC), sheets and ligaments are prone to numerical break-up when their length scales fall below the mesh size. This behavior is consistent with the fact the centerline EPL profile is shifted upstream of the experiment. Adding a thin film model in case 4 allows these small-scale structures to be captured on the mesh, delaying the onset of numerical break-up. Relative to case 3, this shifts the centerline profile downstream and best matches the experiment. Case 4 is further validated by the good agreement shown in the transverse EPL profiles in figure 5.

Using experimental back-lit imaging and equivalent simulation renderings, an intact liquid core length can be extracted [5]. Normalized PDFs of the intact length are shown in figure 6; case 2 qualitatively exhibits a larger mean and kurtosis than the experiment while case 4 shows excellent agreement.

Conclusions

In this study, we present a practical computational strategy for simulating air-blast atomization. We have shown that without the nozzle there exist a strong dependence between the

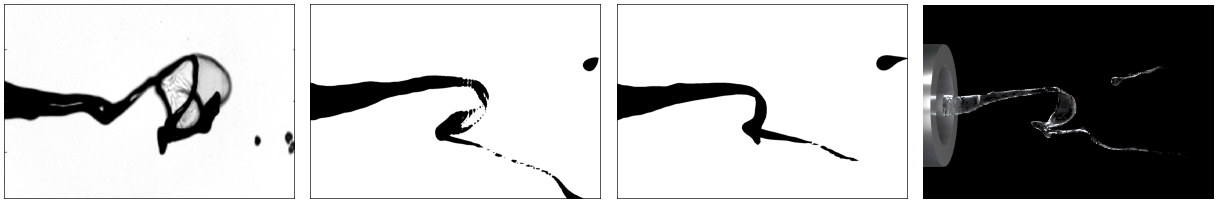

(a) Experimental back-lit image (b) Binarized image using a single plane reconstruction method (c) Binarized image using a thin-film model (d) Ray-traced image using a thin-film model

Figure 4. Thin sheets appear in both experiments (a) and simulations (b-d). Single plane reconstruction methods (b) cannot capture thin-sheets while thin-film models can (c-d).

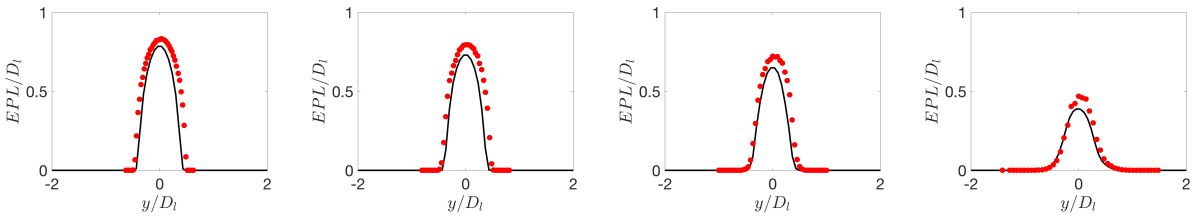

Figure 5. Transverse EPL profiles comparing experiments (•) and case 4 (——) at x/D_l locations of a) 0.18 b) 0.37 c) 0.74 d) 1.48

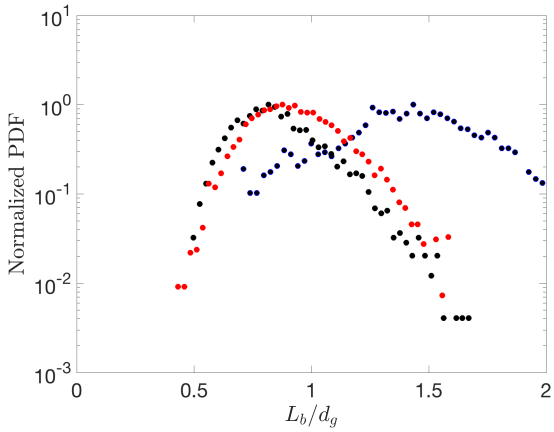

Figure 6. Normalized PDF of intact liquid core length. Experiment (•), Case 2, (•), Case 4 (•).

pinning location of the interface and the resulting centerline EPL profile: pinning to the inside the splitter plate inflates the liquid and shifts the instabilities downstream, while pinning to the outside leads to better agreement with the experiments but a larger liquid intact length. We have also demonstrated that we can get good agreement with experimental EPL data and manage the multi-scale nature of air-blast atomization efficiently by 1) modeling the internal flow of the nozzle with a multi-block strategy, 2) using a dynamic contact line model to allow the interface to travel freely along the splitter plate, and 3) using a thin-film model to delay numerical break-up. Moving forward, we now are in a position to make direct comparisons such as flapping frequency and begin studying the spray dispersion region by transferring resultant drops produced in the atomization simulation, to a third block to be treated as Lagrangian particles. As these simulations are computationally demanding, mesh convergence studies are ongoing work.

Acknowledgements

This work was sponsored by the Office of Naval Research (ONR) as part of the Multidisciplinary University Research Initiatives (MURI) Program, under grant number N00014-16-1-2617. The views and conclusions contained herein are those of the authors only and should not be interpreted as representing those of ONR, the U.S. Navy or the U.S. Government.

A portion of this work was performed at the 7-BM beamline of the Advanced Photon Source, a U.S. Department of Energy (DOE) Office of Science User Facility operated for the DOE Office of Science by Argonne National Laboratory under Contract No. DE-AC02-06CH11357.

Nomenclature

$\langle\cdot\rangle$	Time-averaging operator
Δ	Mesh spacing [m]
d_g	Gas inner diameter [m]
D_g	Gas inner diameter [m]
d_l	Liquid inner diameter [m]
D_l	Liquid inner diameter [m]
EPL	Equivalent path length [m]
κ	Curvature [m^{-1}]
L_b	Intact length [m]
$\mathbf{n}$	Interface normal vector
ρ_g	Gas density [kg m^{-3}]
ρ_l	Liquid density [kg m^{-3}]
σ	Surface tension coefficient [N m^{-1}]
t	Time [s]
μ_g	Gas dynamic viscosity [Pa s]
μ_l	Liquid dynamic viscosity [Pa s]
$\mathbf{u}$	Velocity vector [m s^{-1}]
U_l	Bulk gas velocity [m s^{-1}]
U_g	Bulk liquid velocity [m s^{-1}]
ν_g	Gas kinematic viscosity [$m^2 s^{-1}$]

References

[1] Hopfinger, E. and Lasheras, J., 2004, "Explosive breakup of a liquid jet by a swirling coaxial gas jet," Physics of Fluids, **8**, pp. 1696–1698.

[2] Lasheras, J., Villermaux, E., and Hopfinger, E., 1998, "Break-up and atomization of a round

water jet by a high-speed annular air jet," Journal of Fluid Mechanics, **357**, pp. 351–379.

[3] Marmottant, P. H. and Villermaux, E., 2004, "On spray formation," Journal of Fluid Mechanics, **498**(498), pp. 73–111.

[4] Bothell, J. K., Machicoane, N., Li, D., Morgan, T. B., Aliseda, A., Kastengren, A. L., and Heindel, T. J., 2020, "Comparison of X-ray and optical measurements in the near-field of an optically dense coaxial air-assisted atomizer," International Journal of Multiphase Flow, **125**, p. 103219.

[5] Machicoane, N., Ricard, G., Osuna-orozco, R., Huck, P. D., and Aliseda, A., 2020, "Influence of steady and oscillating swirl on the near-field spray characteristics in a two-fluid coaxial atomizer," International Journal of Multiphase Flow, **129**, p. 103318.

[6] Matas, J.-P., Delon, A., and Cartellier, A., 2018, "Shear instability of an axisymmetric air–water coaxial jet," Journal of Fluid Mechanics, **843**, pp. 575–600.

[7] Hermann, M., 2008, "A balanced force refined level set grid method for two-phase flows on unstructured flow solver grids," Journal of Computational Physics, **227**, pp. 2674–2706.

[8] Fuster, D., Bagué, A., Boeck, T., Le Moyne, L., Leboissetier, A., Popinet, S., Ray, P., Scardovelli, R., and Zaleski, S., 2009, "Simulation of primary atomization with an octree adaptive mesh refinement and VOF method," International Journal of Multiphase Flow, **35**, pp. 550–565.

[9] Gaurav, T., Fuster, S., Daniel Zaleski, and Popinet, S., 2010, "Multiscale simulations of primary atomization," Computers Fluids, **39**, pp. 1864–1874.

[10] Kim, D. and Moin, P., 2010, "Subgrid-scale capillary breakup model for liquid jet atomization," Combustion Science and Technology, **192**, pp. 1334–1357.

[11] Desjardins, O., Blanquart, G., Balarac, G., and Pitsch, H., 2008, "High order conservative finite difference scheme for variable density low Mach number turbulent flows," Journal of Computational Physics, **227**(15), pp. 7125–7159.

[12] Owkes, M. and Desjardins, O., 2014, "A computational framework for conservative, three-dimensional, unsplit, geometric transport with application to the volume-of-fluid (VOF) method," Journal of Computational Physics, **270**, pp. 587–612.

[13] Pilliod, J. E. and Puckett, E. G., 2004, "Second-order accurate volume-of-fluid algorithms for tracking material interfaces," Journal of Computational Physics, **199**(2), pp. 465–502.

[14] Meneveau, C., Lund, T. S., and Cabot, W. H., 1996, "A Lagrangian dynamic subgrid-scale model of turbulence," Journal of Fluid Mechanics, **319**, pp. 353–385.

[15] Chiodi, R., 2020, "Advancement of numerical methods for simulating primary atomization," Doctoral Dissertation, Cornell University.

[16] Wang, S. and Desjardins, O., 2018, "3D numerical study of large-scale two-phase flows with contact lines and application to drop detachment from a horizontal fiber," International Journal of Multiphase Flows, **101**, pp. 35–46.

[17] Popinet, S. and Zaleski, S., 1999, "A front-tracking algorithm for accurate representation of surface tension," International Journal for Numerical Methods in Fluids, **30**, pp. 775–793.